



1 Quantifying the impact of synoptic circulations on ozone 2 variations in North China from April-October 2013-2017

3 Jingda Liu^{1,2}, Lili Wang^{2,3}, Mingge Li^{2,4}, Zhiheng Liao⁵, Yang Sun², Tao Song²,
4 Wenkang Gao², Yonghong Wang³, Yan Li⁶, Dongsheng Ji², Bo Hu², Veli-Matti
5 Kerminen³, Yuesi Wang^{1,2,4,5}, Markku Kulmala³

6 ¹Department of Atmospheric Physics, Nanjing University of Information Science & Technology,
7 Nanjing 210044, China

8 ²State Key Laboratory of Atmospheric Boundary Layer Physics and Atmospheric Chemistry (LAPC),
9 Institute of Atmospheric Physics, Chinese Academy of Sciences, Beijing 100029, China

10 ³Institute for Atmospheric and Earth System Research / Physics, Faculty of Science, University of
11 Helsinki, Finland

12 ⁴University of Chinese Academy of Sciences, Beijing 100049, China

13 ⁵School of Atmospheric Sciences, Sun Yat-sen University, Guangzhou, Guangdong, China

14 ⁶Fangshan Meteorological Bureau, Beijing, 102488, China

15 *Correspondence to:* Lili Wang (wll@mail.iap.ac.cn)

16 **Abstract.**

17 The ozone variation characteristics and the impact of synoptic and local meteorological factors in North
18 China were analysed quantitatively during the warm season from 2013 to 2017 based on multi-city, in-situ
19 ozone and meteorological data, as well as meteorological reanalysis. The domain-averaged maximum
20 daily 8-h running average O₃ (MDA8 O₃) concentration was 122±11 μg m⁻³ with an increase rate of 7.88
21 μg m⁻³ year⁻¹, and the three most highly-polluted months were June (149 μg m⁻³), May (138 μg m⁻³) and
22 July (132 μg m⁻³), which was closely related to synoptic circulation variations. Twenty-six synoptic
23 circulation types (merged into 5 weather categories) were objectively identified using the Lamb-
24 Jenkinson method. The highly-polluted weather categories included S-W-N directions, LP (low-pressure
25 related circulation patterns) and C (cyclone type), and corresponding domain-averaged MDA8 O₃
26 concentration were 122, 126 and 128 μg m⁻³, respectively. Based on the frequency and intensity changes
27 of synoptic circulations, 39.2% of the inter-annual domain-averaged O₃ increase from 2013 to 2017 was
28 attributed to synoptic changes, and intensity of synoptic circulations was the dominant factor. Using
29 synoptic classification and local meteorological factors, the segmented synoptic-regression approach was
30 established to evaluate and forecast daily ozone variations on an urban scale. The results showed that
31 this method is practicable in most cities, and that the dominant factors are the maximum temperature,
32 southerly winds, relative humidity in the previous and in the same day, and total cloud cover. Overall,
33 43~64% of the day-to-day variability of MDA8 O₃ concentrations was due to local meteorological
34 variations in most cities over North China, except for QHD~32% and ZZ~25%. Our quantitative
35 exploration on synoptic and local meteorological factors influencing both on inter-annual and day-to-day
36 ozone variations will provide the scientific basis for evaluating emission reduction measures, since the
37 national and local governments have implemented a series of measures to mitigate air pollution in North
38 China in these five years.



39 1 Introduction

40 Tropospheric ozone (O_3) is one of the air pollutants of the greatest concern due to its significant harm to
41 human health and vegetation (Kinney, 2008; Jacob and Winner, 2009; Knowland et al., 2017), and it is
42 formed through the nonlinear interactions between NO_x and volatile organic compounds in combination
43 with sunlight (Liu et al., 2007; Liu et al., 2012). Thus, ozone levels are controlled by precursors and
44 meteorological conditions. With industrialization advancement and rapid economic growth, North China
45 is one of the most populated and most polluted regions in the world. Although the national and local
46 governments have implemented a series of measures to reduce emissions since 2013, $PM_{2.5}$ decreased
47 significantly, whereas O_3 pollution is still serious in this region (Lu et al., 2018; Li et al., 2019). Several
48 studies have explored the variation of summer ozone in China (Lu et al., 2018; Li et al., 2019), but
49 systematic research aiming at quantifying the evolution characteristics of ozone and meteorological
50 impact and contribution are still lacking for the whole warm season (April-October) in the five years
51 (2013-2017) during which Action Plan for Air Pollution Prevention and Control (APAPPC) was
52 implemented. This is an undesired situation if we want to understand the effect of emission reduction
53 measures on ozone in North China.

54 Meteorological factors affect ozone levels through a series of complex process combinations,
55 including emission, transport, chemical transformations and removal (Chan and Yao, 2008).
56 Meteorological conditions are the primary factor determining day-to-day variations in pollutant
57 concentrations over China (He et al., 2016; He et al., 2017), whereas long-term O_3 trends are influenced
58 both by climatological (circulation types, temperature, humidity, and radiation, etc.) and environmental
59 factors (changes in anthropogenic and natural sources). Therefore, the impact of reduced anthropogenic
60 emissions on O_3 variation can be estimated more accurately if we are able to quantify the meteorological
61 influence.

62 Synoptic meteorological conditions have an important effect on the regional ozone distribution and
63 variation (Shen et al., 2015). One typical synoptic circulation represents a relatively homogeneous
64 meteorological condition, so synoptic classification is useful for getting insight into the impact of
65 meteorology on ozone levels in a regional scale. Previous studies have proved a significant connection
66 between the weather type and surface O_3 concentration, but the relation between these two quantities
67 varies in different regions in associating with differences in the topography, pollution source, local
68 circulation, etc (Hegarty et al., 2007; Demuzere et al., 2009; Zhang et al., 2012; Zhang et al., 2013; Pope
69 et al., 2016; Liao et al., 2017). For example, based on the Lamb-Jenkinson weather typing technique,
70 Demuzere et al. (2009) demonstrated higher surface O_3 concentrations in summer in an easterly weather
71 type at a rural site in Cabauw, Netherlands, whereas an opposite result was obtained by Liao et al. (2017)
72 in the Yangtze River Delta region in eastern China. Therefore, synoptic classification and its relationship
73 with O_3 need to be explored separately in different regions. In addition, based on synoptic classification,
74 Comrie and Yarnal (1992) and Hegarty et al. (2007) suggested a reconstructed pollutant concentration
75 (caused by synoptic influence) algorithm, which can separate climatological and environmental
76 variability in environmental data. It was found that 46% and 50% of the inter-annual variability in the O_3
77 concentration was reproduced in Northeast America (Hegarty et al., 2007) and Hong Kong (Zhang et al.,
78 2013), respectively, by taking into account the inter-annual changes in the frequency and intensity of
79 synoptic patterns.

80 In an urban scale, the daily variation of ozone is affected by both synoptic and local meteorological
81 factors. Clarifying and quantifying this relationship is vital and helpful for daily ozone pollution potential
82 forecasts and for quantifying the contribution of local meteorological factors to the day-to-day variation



83 of ozone, which will provide scientific basis and guidance for making reasonable ozone reduction
84 measures. A weather type classification prior to the regression analysis is superior to a simple linear
85 regression approach (Eder et al., 1994; Barrero et al., 2006; Demuzere et al., 2009; Demuzere and van
86 Lipzig, 2010), and the synoptic-regression-based algorithm can reproduce the observed O₃ distributions
87 and provide a better parameterization to facilitate understanding of ozone's dependence on meteorology
88 in certain urban region.

89 Overall, in this study, we explore how the maximum daily 8-h running average O₃ (MDA8 O₃)
90 concentration varies and quantify the contribution of synoptic and local meteorological conditions on
91 ozone variations in North China (58 cities covering Hebei, Shanxi, Shandong, and Henan Provinces, the
92 Beijing and Tianjin municipalities) from April-October 2013-2017. Our specific goals are 1) to
93 demonstrate characteristics and variation trend in surface MDA8 O₃ concentration, 2) to find out the
94 predominant synoptic circulations and meteorological mechanism for regional ozone levels and
95 variability, 3) to quantify the contribution of circulation changes (frequency and intensity) to the inter-
96 annual variability of the O₃ concentration, 4) to identify the prominent meteorological variables and
97 construct the O₃ potential forecast model in main cities, and quantify the contribution of local
98 meteorological factors to the day-to-day variation in O₃ levels.

99 2 Data and methods

100 2.1 Ozone and PM_{2.5} data

101 The hourly O₃ and PM_{2.5} data during April-October, 2013-2017 were derived from the National Urban
102 Air Quality Real-time Publishing Platform (<http://106.37.208.233:20035/>). According to technical
103 regulation for ambient air quality assessment (HJ 663-2013, <http://www.mee.gov.cn/>), the MDA8 O₃
104 concentration was calculated for each monitoring site based on the hourly data from 08:00-24:00 for
105 the days with no <14-h measurements. If there is less than 14 hours of valid data, the results are still
106 valid if the MDA8 O₃ concentration exceeds the national concentration limit standard. Each city has at
107 least two monitoring sites and the city ozone levels are the corresponding averages over all the sites in
108 that city. Ozone data were collected in only 14 cities for the time period 2013-2017 and in additional 44
109 cities for the time period 2015-2017, with detailed information shown in Fig. 1 and table S1. The
110 original unit of the ozone observations is µg/m³, and the converted coefficient from mixing ratios (unit:
111 ppbv) to µg/m³ is a constant (e.g. 0.5 at temperature of 25 °C and pressure of 1013.25 hPa). In this
112 study, we will use the original unit. If not otherwise mentioned, the analysis of O₃ refers to the time
113 period April-October in this paper.

114 2.2 Meteorological data

115 Gridded-mean sea level pressure data, 10 metre U and V wind component (U₁₀, V₁₀, respectively),
116 boundary layer height (BLH) and 2-metre temperature (T₂) with a 1° horizontal resolution and vertical
117 velocity (ω) from 1000-100 hPa (27 levels) and wind divergence (div) from 1000-850 hPa (7 levels) in
118 6-h intervals (Beijing time 02, 08, 14 and 20) for 2013-2017 were obtained from the European Centre
119 for Medium Weather Forecast Re-analysis Interim (ERA-Interim).

120 Four measurements per day for temperature (T), relative humidity (RH), total cloud cover (TCC), rain,
121 wind speed (ws) and direction (wd), pressure (pre) in 58 cities during April-October in 2013-2017 were
122 obtained from China Meteorological Administration in the Meteorological Information Combine



123 Analysis and Process System (MICAPS). Then daily-mean meteorological factors were averaged from
124 four measurement (scalar averaging for most factors, whereas vector averaging for wind speed and wind
125 direction which means using u component (U) and v component (V) for averaging). The meteorological
126 station with a minimum distance from the city center was chosen.

127 **2.3 Lamb-Jenkinson circulation typing**

128 The Lamb-Jenkinson weather type approach (Lamb, 1972; Yarnal, 1993; Trigo and Dacamara, 2000;
129 Demuzere et al., 2009; Russo et al., 2014; Santurtún et al., 2015; Pope et al., 2016; Liao et al., 2017) was
130 widely employed to classify the synoptic circulation, which uses coarsely gridded pressure data on a 16-
131 point moveable grid where North China is set as the center. The 16-point grid, North China and 58 major
132 cities are shown in Fig. 1a. The daily mean sea level pressure data are averaged among four time points
133 to determine the daily weather type. The detailed classification procedure can be found in Trigo and
134 Dacamara (2000).

135 **2.4 Reconstruction of O₃ concentration based on the synoptic classification**

136 To quantify the interannual variability captured by the surface circulation pattern variations, Comrie and
137 Yarnal (1992) suggested an algorithm to separate synoptic and non-synoptic variability in environmental
138 data, by multiplying the overall mean value of a particular pattern by the occurrence frequency of that
139 type of year, the climate signal could be obtained as follows:

$$140 \quad \overline{\overline{O_3}}_m(\text{fre}) = \sum_{k=1}^{26} \overline{O_3}_k F_{km} \quad (1)$$

141 Here $\overline{\overline{O_3}}_m(\text{fre})$ is the reconstructed mean MDA8 O₃ concentration influenced by frequency changes of
142 circulation patterns during April-October for the year m, $\overline{O_3}_k$ is the 5-year mean MDA8 O₃
143 concentration per circulation pattern k, and F_{km} is the occurrence frequency of circulation pattern k
144 during April-October for the year m.

145 Hegarty et al. (2007) suggested that variations in the circulation pattern are attributed not only to
146 frequency changes but also to intensity variations, and that considering these two changes can better
147 separate environmental and climate-related contributions in the inter-annual ozone variation. As a result,
148 Equation (1) is modified into the following form:

$$149 \quad \overline{\overline{O_3}}_m(\text{fre} + \text{int}) = \sum_{k=1}^{26} (\overline{O_3}_k + \Delta O_{3km}) F_{km} \quad (2)$$

150 where $\overline{\overline{O_3}}_m(\text{fre} + \text{int})$ is the reconstructed mean MDA8 O₃ concentration influenced by the frequency
151 and intensity changes of circulation patterns during April-October for the year m, ΔO_{3km} is the modified
152 difference which is on the fitting line, obtained through a linear fitting of the annual MDA8 O₃
153 concentration anomalies (ΔO_3) to the circulation intensity index (CII) for circulation pattern k in the year
154 m. ΔO_{3km} represents the part of annual observed ozone oscillation caused by the intensity in each
155 circulation pattern. Hegarty et al. (2007) used the domain-averaged sea level pressure (mslp) representing
156 CII.

157 To better characterize intensity variations, we added 5 circulation intensity indexes: the difference
158 between the highest pressure and lowest pressure (gradient), the center pressure of the highest pressure
159 system (max slp), the center pressure of the lowest pressure system (min slp), the distance from the
160 highest pressure centres to the study city (dis max), and the distance from the lowest pressure centres to
161 the study city (dis min). The effective circulation intensity index (ECII) is one of the 6 CIIs, which has



162 the strongest correlation coefficient (r) between CII and ΔO_3 . Thus, ECII is used in equation (2) to
163 calculate ΔO_{3km} . All CIIs for 14 cities were calculated based on $10^\circ \times 10^\circ$ grids covering North China
164 ($32^\circ N$ - $42^\circ N$, $110^\circ E$ - $120^\circ E$). One example of ΔO_{3km} (circulation pattern C in ZJK) is shown in Fig. 7a.
165 Min slp has the largest r (-0.97) among 6 CIIs in type C in ZJK, therefore, min slp is the ECII.

166 2.5 The segmented synoptic-regression approach and model validation

167 The utilization of a segmented synoptic-regression approach could aid in minimizing the errors when
168 using linear regression to model a nonlinear relationship and effectively forecast ozone variation
169 (Robeson and Steyn, 1990; Liu et al., 2007; Demuzere and van Lipzig, 2010; Liu et al., 2012). Based on
170 local monitored meteorological data, their 24-h time lag values and weather type classifications, stepwise
171 linear regression was used in every weather category to construct the ozone potential forecast model. The
172 detail of main methods is shown in the Text S1.

173 Statistical model performances were evaluated by the following factors: R^2 (variance in the individual
174 model's coefficients of determination); rmse (root mean square error); CV (coefficient of variation
175 defined as $rmse/\text{mean MDA8 } O_3$). All statistics are based on MATLAB R2015b.

176 3. Results and discussion

177 3.1 Characteristics and variation trend of ozone concentrations in North China

178 The MDA8 O_3 concentration is one of six factors in calculating the daily air-quality index in China. Five
179 ranks are separated, representing different air-quality levels, and these are excellent, good, lightly
180 polluted, moderately polluted and heavily polluted days with cut off concentrations of 100, 160, 215 and
181 $265 \mu\text{g m}^{-3}$. The Grade II National Ambient Air Quality Standard for the daily limit is $160 \mu\text{g m}^{-3}$. The
182 spatial distribution of the averaged MDA8 O_3 concentration (Fig. 1b) and exceedance ratio (Fig. 1c), and
183 detailed information in the 58 cities (Table S1), show a severe ozone pollution problem during the recent
184 five years in North China. The domain-averaged MDA8 O_3 concentration for 58 cities was $122 \pm 11 \mu\text{g m}^{-3}$
185 with an increasing rate of $7.88 \mu\text{g m}^{-3} \text{ year}^{-1}$ and exceedance ratio was $22.2 \pm 8.2\%$. Notably, the most
186 polluted cities are concentrated in Beijing, the southeast of Hebei and the west and north of Shandong,
187 where the averaged MDA8 O_3 concentration was $130 \pm 9 \mu\text{g m}^{-3}$ and exceedance ratio was $27.9 \pm 7.2\%$.

188 The daily evolution of MDA8 O_3 concentrations during 2013-2017 in 14 cities (Fig. 2a) indicates
189 periodical, consistent and regional characteristics for ozone pollution. The most highly-polluted periods
190 are from mid-May to mid-July. Especially in 2017, the frequency and level of ozone pollution increased
191 significantly, and regional persistent ozone pollution events increased. The rate of the MDA8 O_3
192 concentration increase during 2013-2017 was $0.87 \mu\text{g m}^{-3} \text{ month}^{-1}$ (Fig. 2b), and this growth was
193 accompanied by a decreasing trend of the $PM_{2.5}$ concentration (Fig. S1). The reduction of the particle's
194 extinction for sunlight due to the declined $PM_{2.5}$ concentration can lead to an increase in radiation
195 reaching the ground; in addition, Li et al. (2019) suggested that decrease of $PM_{2.5}$ slowed down the
196 aerosol sink of hydro-peroxyl (HO_2) radicals and thus stimulated ozone production. Thus, the rise in
197 ozone is partly due to the decline in $PM_{2.5}$. Overall, the annual domain-averaged MDA8 O_3
198 concentrations for 58 cities were 102, 109, 116, 119 and $136 \mu\text{g m}^{-3}$ in 2013, 2014, 2015, 2016 and 2017,
199 respectively (Fig. 3a). The exceedance ratios for all cities were found to be 12.9%-19.4% during 2013 to
200 2016, but reached 31.1% in 2017.



201 The monthly-mean MDA8 O₃ concentrations (Fig. 3b) from April-October were 112, 138, 149, 132,
202 124, 117 and 75 µg m⁻³, respectively, and the corresponding exceedance ratios were 9.4, 30.1, 41.1, 26.1,
203 20.3 20.1 and 3.3%. The highest domain-averaged MDA8 O₃ concentration and exceedance ratio
204 occurred in June, followed by May, July, August, September, April and October. Meteorological
205 conditions led to high ozone concentrations in June, and monsoon circulation in July and August resulted
206 in cloudy, rainy and less radiation in the study area (Wang et al., 2009b; Tang et al., 2012). The higher
207 ozone concentrations in April compared with October could be associated with strong winds, resulting
208 in ozone downward transport due to the lower stratosphere folding mechanism (Delcloo, 2008; Demuzere
209 et al., 2009; Tang et al., 2012). Remarkably, the conclusion is different from Tang et al. (2012). The
210 domain-averaged MDA8 O₃ in May was even higher than in July, the concentrated pollution episode
211 occurred earlier, especially in 2017. The second half of May was the most polluted period and the
212 exceedance ratio was 46.1%, which is higher than those observed in the first half of June (39.5%), the
213 second half of June (45.4%) and the first half of July (35.6%). The reason for this is probably the
214 abnormally higher temperatures in May, especially the second half of May, during 2013-2017 and
215 particularly in 2017 (Fig. S2). Many researches have found a strong positive correlation between ozone
216 levels and temperature (Eder et al., 1994; Demuzere et al., 2009; Zhang et al., 2012; Ma et al., 2016; He
217 et al., 2017).

218 3.2 Circulation patterns and associated surface O₃ levels

219 3.2.1 Predominant circulation patterns and corresponding meteorological conditions and regional 220 ozone concentrations

221 Based on the Lamb-Jenkinson weather typing technique, 26 circulation patterns affecting North China
222 were identified, including two vorticity types (anticyclone, A and cyclone, C), eight directional types
223 (northeasterly, NE; easterly, E; southeasterly, SE; southerly, S; southwesterly, SW; westerly, W;
224 northwesterly, NW; and northerly, N) and 16 hybrids of vorticity and directional types (CN, CNE, CE,
225 CSE, CS, CSW, CW, CNW, AN, ANE, AE, ASE, AS, ASW, AW, and ANW). The composite mean sea
226 level pressure maps, along with the occurrence days are shown in Fig. 4. The obvious positional
227 differences of the high- and low-pressure centres have been shown in the different weather types resulted
228 in different meteorological variables. The occurrence ratios of vorticity types, pure directional types, and
229 the hybrid types were 35.6%, 38.8% and 25.6% in all 1070 days, respectively.

230 The mid-latitude eastern Eurasian continent is strongly affected by monsoon circulation, and there are
231 several key synoptic systems affecting the circulation and meteorological conditions in North China.
232 During our study period, North cyclones (Mongolian and Yellow River cyclone), indicative of a low-
233 pressure located in the northwest of North China, dominate in spring and summer. Siberian high
234 influences the northern China in spring and autumn. Western Pacific Subtropical High is also a key
235 system in summer. Therefore, these main synoptic systems result in frequency variations of circulation
236 types in different months over North China.

237 According to the different locations of the different central systems, together with the similar
238 meteorological factors and mean MDA8 O₃ values in these circulations, 26 circulation types were merged
239 into 5 weather categories: 1) N-E-S direction including N, NE, E, SE, AN, ANE, AE and ASE; 2) S-W-
240 N direction including S, SW, W, NW, AS, ASW, AW and ANE; 3) LP (low-pressure related circulation
241 patterns) including CN, CNE, CE, CSE, CS, CSW, CW and CNW; 4) A (anticyclone) and 5) C (cyclone).
242 The occurrence ratios of 5 weather categories were 25.4%, 26.5%, 12.5%, 17.5% and 18.1% in all 1070



243 days, respectively. The predominant local meteorological conditions associated with a specific weather
244 category play an important role in ozone pollution, influencing ozone photoreaction or its regional
245 transport. The statistical values of averaged MDA8 O₃ concentration, frequency of circulations and
246 meteorological variables are depicted in Table 1 and Fig. 5. Briefly, the N-E-S direction and A categories
247 were typically associated with cool and wet air, moderate rain and TCC, low BLH, as well as relative
248 clean air masses from the region of the inner-Mongolia/eastern ocean (Fig. S3), which is unfavourable
249 for ozone formation, and the corresponding area-averaged MDA8 O₃ concentration were 98±6 μg m⁻³
250 and 96 μg m⁻³, respectively. The S-W-N direction category with moderate T and BLH, lower RH, weak
251 wind, sporadic clouds and rain, and stronger subsidence in low troposphere contributed to higher ozone
252 levels (122±8 μg m⁻³). The highest ozone concentrations (126±16 and 128 μg m⁻³) were related to LP and
253 C categories, respectively, which can probably be attributed to favourable meteorological conditions (hot
254 and humid air, a small amount of TCC and rainfall, and high BLH) for ozone formation and transport.
255 However, CE and CSE are different from the other circulation types in the LP category, with lower O₃
256 concentration due to lower temperatures and easterly winds from the ocean. Overall, the peak values of
257 ozone always occurred in the front of the cold frontal passage or cyclone (most circulation types in LP,
258 and C), whereas the valley values exhibited during or after the cold frontal passage (most circulation
259 types in the N-E-S direction, C with heavy rainfall and CE).

260 3.2.2 Spatial distributions of the 26 circulation types/five categories

261 The spatial distribution of the averaged MDA8 O₃ concentration under different weather types is shown
262 in Fig. 6, and Figs. S3-S7 display the spatial distributions of the combined wind field with BLH,
263 maximum temperature (T_{max}), RH, rain and TCC, respectively. In most cities, the lowest MDA8 O₃
264 concentrations occurred in the weather categories N-E-S direction and A. The S-W-N direction category,
265 having predominantly southerly winds in the whole or south of North China, exhibited a high-value
266 ozone along with the prevailing wind direction. The LP and C weather categories, having the highest
267 regional averaged levels, were associated with high T_{max} and strong southerly flow, moderate RH and
268 ample sunshine, which provides favourable meteorological conditions for ozone formation as well as
269 ozone and its precursors transport from the polluted area.

270 3.2.3 Inter-annual/monthly ozone variation elaborated from the perspective of circulation change

271 The inter-annual or monthly ozone concentration changes are associated with variations in circulation
272 types. Figure 3 indicates that the ratios of high-ozone weather categories (S-W-N direction, LP and C S-
273 W-N direction, LP and C) were most frequent in 2013 and 2017, less frequent in 2015 and 2016, and
274 least frequent in 2014. The high-ozone weather categories accounted for 61.5% and 61.8% of the time
275 in 2013 and 2017, respectively. In similar weather conditions, lower ozone levels could be also associated
276 with higher PM_{2.5} levels in 2013 and 2015. Quantifying the contribution of frequency-only and
277 circulation changes (frequency and intensity) to the inter-annual variability of ozone will be discussed in
278 Section 3.3.

279 Affected by monsoon circulation systems, the frequencies of weather types vary dramatically on a
280 monthly scale (Fig. 3b). The frequencies of both N-E-S direction and A decrease gradually in spring,
281 whereas the frequencies of the S-W-N direction, LP and C gradually increase. In autumn, the frequencies
282 of LP and C decrease, whereas those of S-W-N direction, N-E-S direction and A increase. The weather
283 categories C and LP dominate in summer. The high-ozone weather categories (S-W-N direction, LP and



284 C) accounted for 58.7, 66.5, 79.3, 80.6, 49.0, 38.0 and 27.7% of the time in April to October, respectively.
285 These frequencies were highest in July, Jun, and May, which probably resulted in highest monthly-
286 averaged regional ozone concentrations. However, due to the influence of monsoon circulation in July,
287 large amounts of rainfall occurred during this month: 73 out of 194 days during the 5 years were rainy
288 in category C, which reduced ozone levels. Notably, severe ozone pollution in May and especially in the
289 second half of May in 2017 is closely related to abnormally high frequency under the control of most-
290 polluted synoptic categories (LP and C), account for 35.5% in 31days and 50.0% in 16 days, respectively
291 (Table S2). With the development of Siberian high from August to October, the weather categories N-
292 E-S direction and A occurred frequently, and monthly-averaged ozone concentrations declined.

293 3.3 Effects of synoptic changes on the inter-annual ozone variations

294 3.3.1 Effect of circulation intensity on inter-annual ozone variations

295 The pressure fields for 26 synoptic types per year during 2013-2017 (Fig. S6) show that every synoptic
296 circulation type varies in both of frequency and intensity. The intensity of circulation variations indicates
297 the difference of the center pressure, the location of predominant system, pressure gradient, and domain-
298 averaged sea level pressure. There were different correlations between ECII and ΔO_3 (as introduced in
299 Section 2.4) in different circulation types for different cities. For instance, the strong negative correlation
300 between these two variables for the circulation type C in ZJK (Fig. 7a) indicates that lower values of min
301 slp were associated with higher MDA8 O_3 concentrations.

302 The number of cities and averaged r according to corresponding ECII under each circulation type
303 among 14 cities are shown in Fig.7b. Overall, the averaged absolute value of r was 0.74. For the
304 circulation type C, ΔO_3 correlated with min slp best in 9 of the cities, and the averaged r was -0.81, i.e.
305 a strong negative correlation. A strong negative correlation between ΔO_3 and pressure gradient is
306 evident for the circulation type N, whereas an opposite pattern occurs for circulation types CSE and CS.
307 The reasons for this difference are as follows. Northerly winds are prevailing for type N, and a high
308 pressure gradient means strong northerly winds bringing clean air mass from the north, which results in
309 a decrease in the MDA8 O_3 concentration. However, high temperatures and RH as well as prevailing
310 southerly or easterly winds (Fig. S3-5) occur in southern cities in type CSE or CS. In addition, the
311 abundance of precursors and ozone in the upwind region facilitate ozone formation and transport with
312 the increasing pressure gradient (wind speeds).

313 Even under the same circulation controls, the ECII and the value of r in different cities are different.
314 This phenomenon is caused by the differences of geographic location, topographic discrepancy, and the
315 properties of the upwind air mass, etc. Therefore, under the control of same circulation type, the ECII of
316 adjacent cities is the same.

317 3.3.2 Quantifying the effects of the inter-annual synoptic changes on the inter-annual ozone 318 variations

319 Based on equations (1) and (2), we reconstructed the inter-annual ozone levels by taking into account
320 either frequency-only or both frequency and intensity variations of synoptic circulations, which are
321 $\overline{O_{3m}}(\text{fre})$ and $\overline{O_{3m}}(\text{fre} + \text{int})$, respectively. The difference between maximum and minimum annual
322 reconstructed ozone is labelled as $\Delta \overline{O_{3m}}(\text{fre})$ and $\Delta \overline{O_{3m}}(\text{fre} + \text{int})$, respectively. $\Delta O_{3\text{-obs}}$ is different
323 between maximum and minimum for annual observed O_3 concentration. Thus, the contributions of inter-
324 annual variability in O_3 influenced by frequency-only and by frequency and intensity variation of



325 synoptic circulation are $\overline{\Delta O_{3m}}(\text{fre})/\Delta O_{3_obs}$ and $\overline{\Delta O_{3m}}(\text{fre} + \text{int})/\Delta O_{3_obs}$, respectively, which
326 indicates the inter-annual ozone levels oscillation caused by synoptic variability.

327 The observed and reconstructed (influenced by frequency-only and by frequency and intensity
328 variations of synoptic circulations) inter-annual MDA8 O₃ levels for 5 years in 14 cities and the whole
329 region are shown in Fig. 8. The contribution of inter-annual variability in O₃ influenced by frequency
330 and intensity variation of synoptic circulation ranged from 44.1 to 69.8% over the 14 cities, and the
331 contribution by the frequency-only variation ranged from 5.2 to 23.4%. Obviously, the inter-annual
332 fluctuation of the ozone concentration is caused mainly by weather type intensity changes in North China.
333 In addition, based on regional averaged scale, inter-annual variability in domain-averaged observed
334 MDA8 O₃ in 14 cities varied from averaged maximum values 135 μg m⁻³ in 2017 to a minimum 104 μg
335 m⁻³ in 2013. The contributions of circulation variations on inter-annual O₃ increase was 39.2%, and the
336 remaining inter-annual variability was possibly due to nonlinear relationships with recent emission
337 control measures over North China.

338 Our results (44.1~69.8%) are higher than that (50%) of Zhang et al. (2013) in most cities. The
339 difference could be attributed to our result based on (1) more weather types, (2) weather types covering
340 all days, (3) more CIIs which can better characterize intensity. Furthermore, a higher contribution in
341 single city and increasing reconstructed ozone indicate that synoptic circulations play an important role
342 in ozone variations in North China. But our regional result (39.2%) is lower than that (46%) of Hegarty
343 et al. (2007), which reveals that the increasing trend for ozone from 2013 to 2017 in North China is
344 associated with the impact of its precursors to a large extent.

345 3.4 Forecasting O₃ levels using a segmented synoptic-regression approach

346 Based on five weather categories defined in section 3.2.1, a segmented synoptic-regression analysis
347 approach (introduced in section 2.5) was established to construct the ozone potential forecast model. The
348 results of segmented synoptic-regression analysis in 14 cities, i.e. the daily MDA8 O₃ potential forecast
349 equations for each category in each city, are shown in Table S3. Table 2 represents the number of cities
350 (in total 14) from which the meteorological factors were used in a stepwise regression model under each
351 weather category. The results show that T_{max} shows a strongly positively correlation with ozone, being
352 the primary influencing factor in all categories and all cities: high temperatures are related to large ozone
353 concentrations in North China. V shows a positive correlation with O₃ in the northern part of this region
354 (around 38.5°N as the North-South boundary), which means that the southerly flow causes an increase
355 in ozone concentration. Therefore, as discussed in Section 3.2.2, high temperatures and southerly winds
356 are the main factors contributing to increased ozone concentrations in North China from a regional
357 perspective. Both RH_{lag} and RH show a negative correlation with O₃, and the former has more
358 occurrences and weight in equations. This could be because a proper moisture which is around 40-50%
359 (Zhao et al., 2019) generates more hydroxyl radicals (OH) facilitating ozone formation; and ozone is
360 stored in the residual layer and is transported into the surface during the next day by convection and
361 diffusion. In addition, TCC is also a key factor.

362 Three statistic factors (R², rmse, and CV) for building and validation datasets for 5 weather categories
363 and composite model in 14 cities (Table S4) indicated that the potential forecast equations of MDA8 O₃
364 in most cities are acceptable. R² was higher than 0.50 except for QHD, SJZ, HD and ZZ (0.27-0.46),
365 while CV was lower than 40%, except for TY and ZZ. For the validation dataset, scatter plots of predicted
366 versus observed MDA8 O₃ concentrations in composite validation datasets in each city are shown in Fig.
367 9. The results reveal that most of the validation data are in the acceptable error range within the 2:1 and



368 1:2 ratio lines, and the scatters are distributed evenly around the 1:1 line. This also indicates that the
369 segmented synoptic-regression approach is practicable to construct the ozone potential forecasting model
370 in most cities in North China.

371 In addition, the contribution of local meteorological factors to the day-to-day variation of ozone can
372 be evaluated by the explained variance (R_E^2) calculated from the synoptic-regression-based models (Hien
373 et al., 2002; Wang et al., 2009a). Overall, as shown in Fig. 9, local meteorological parameters could
374 explain 55-64% and 43-49% of the day-to-day MDA8 O₃ concentration variations for the north cities
375 (except for QHD, 32%) and south cities (except for ZZ, 25%), respectively.

376 In brief, the aforementioned results can provide references for daily MDA8 O₃ prediction for each city
377 and facilitate understanding and cognizing the impact of local meteorology on daily ozone variation on
378 urban scale.

379 4 Conclusions

380 In this study, we demonstrated inter-annual/monthly variation in the surface MDA8 O₃ concentration in
381 North China during April-October 2013-2017, investigated the relationship between weather types and
382 MDA8 O₃ levels, quantified the contribution of weather types and local meteorological factors variations
383 on both inter-annual and day-to-day variability of ozone, and built the ozone potential forecast equations.
384 The main results are as follow:

385 1. The annual domain-averaged concentrations of MDA8 O₃ during 2013-2017 were 102, 109, 116,
386 119, and 136 $\mu\text{g m}^{-3}$, respectively, and highest exceedance ratio (31.1%) was observed in 2017. The
387 monthly mean MDA8 O₃ concentrations were 112, 138, 149, 132, 124, 117, and 75 $\mu\text{g m}^{-3}$ in April to
388 October, respectively, with a significantly increasing rate of 0.87 $\mu\text{g m}^{-3} \text{ month}^{-1}$ during the five-year
389 period. The most polluted cities are concentrated in Beijing, the southeast of Hebei and the west and
390 north of Shandong.

391 2. Twenty-six weather types were objectively identified based on the Lamb-Jenkinson method, and
392 combined into five weather categories due to similar meteorological factors and MDA8 O₃
393 concentrations. The high ozone levels in 2017, and during May-July, were partly due to the high
394 frequency of the highly-polluted weather categories (S-W-N direction, LP and C) due to high
395 temperatures, moderate RH and southerly air flows.

396 3. Intensity of synoptic circulation is the dominant factor which caused the impact of weather types
397 variations on ozone levels variations. The contribution of inter-annual variability in O₃ influenced by
398 both frequency and intensity variations of synoptic circulation ranged from 44 to 70% over the 14 cities
399 considered in detail, whereas the contributions of circulation variations on inter-annual O₃ increase from
400 2013 to 2017 was only 39.2% based on regional averaged scale.

401 4. The results of daily ozone potential forecast equations in the 14 cities shows that high temperatures,
402 moderate RH and south winds could result in severe ozone pollution in the northern part of North China,
403 whereas the southern part is affected mainly by high temperatures and RH. Local meteorological
404 parameters could explain 55-64% and 43-49% of the day-to-day MDA8 O₃ variations for the north cities
405 (except for QHD, 32%) and south cities (except for ZZ, 25%), respectively.



406 **Author contribution**

407 LL Wang designed this research. JD Liu and LL Wang interpreted the data and wrote the paper. MG Li
408 processed some of the data. The weather type classification program was provided by ZH Liao. Y Sun,
409 T Song, and WK Gao provided some of the PM_{2.5} and O₃ data. Y Li provided some of the meteorological
410 data. All of the authors commented on the paper.

411 **Data availability**

412 Daily average mass concentrations of ozone were obtained from the National Urban Air Quality Real-
413 time Publishing Platform (<http://106.37.208.233:20035/>) issued by the Chinese Ministry of Ecology and
414 Environment. Daily meteorological data were obtained from the China Meteorological Administration
415 in the Meteorological Information Combine Analysis and Process System (MICAPS), and daily
416 meteorological reanalysis data (gridded at 1°× 1°) were obtained from ERA-Interim
417 (<https://apps.ecmwf.int/datasets/data/interim-full-daily/levtype=sfc/>). All of the data can be obtained
418 upon request.

419 **Competing interests**

420 The authors declare that they have no conflict of interest.

421 **Acknowledgments**

422 This work was partially supported by grants from the National Key R&D Plan (Quantitative Relationship
423 and Regulation Principle between Regional Oxidation Capacity of Atmospheric and Air Quality
424 2017YFC0210003), the National Natural Science Foundation of China (No. 41505133 & 41775162), the
425 National Research Program for Key Issues in Air Pollution Control (DQGG0101) and a program of the
426 China Scholarships Council. We give special thanks to the National Earth System Science, Data Sharing
427 Infrastructure, and the National Science & Technology Infrastructure of China.

428 **References**

- 429 Barrero, M. A., Grimalt, J. O., and Cantón, L.: Prediction of daily ozone concentration maxima in the
430 urban atmosphere, *Chemometrics and Intelligent Laboratory Systems*, 80, 67-76,
431 10.1016/j.chemolab.2005.07.003, 2006.
- 432 Chan, C. K., and Yao, X.: Air pollution in mega cities in China, *Atmospheric Environment*, 42, 1-42,
433 10.1016/j.atmosenv.2007.09.003, 2008.
- 434 Comrie, A. C., and Yarnal, B.: Relationships between synoptic-scale atmospheric circulation and ozone
435 concentrations in Metropolitan Pittsburgh, Pennsylvania, *Atmospheric Environment, part B, urban
436 Atmosphere*, 26, 301-312, 1992.
- 437 Delcloo, A. W. a. D. B., H.: Five day 3D back trajectory clusters and trends analysis of the Uccle ozone
438 sounding time series in the lower troposphere (1969–2001), *Atmos. Environ.*, 42, 4419–4432, 2008.



- 439 Demuzere, M., Trigo, R. M., Vila-Guerau de Arellano, J., and van Lipzig, N. P. M.: The impact of
440 weather and atmospheric circulation on O₃ and PM₁₀ levels at a rural mid-latitude site, *Atmos. Chem.*
441 *Phys.*, 9, 2695-2714, <https://doi.org/10.5194/acp-9-2695-2009>, 2009.
- 442 Demuzere, M., and van Lipzig, N. P. M.: A new method to estimate air-quality levels using a synoptic-
443 regression approach. Part I: Present-day O₃ and PM₁₀ analysis, *Atmospheric Environment*, 44, 1341-
444 1355, <https://doi.org/10.1016/j.atmosenv.2009.06.029>, 2010.
- 445 Eder, B. K., Davis, J. M., and Bloomfield, P.: An Automated Classification Scheme Designed to Better
446 Elucidate the Dependence of Ozone on Meteorology, *J.appl.meteor.*, 33, 1182-1199, 1994.
- 447 He, J., Yu, Y., Xie, Y., Mao, H., Wu, L., Liu, N., and Zhao, S.: Numerical Model-Based Artificial Neural
448 Network Model and Its Application for Quantifying Impact Factors of Urban Air Quality, *Water, Air, &*
449 *Soil Pollution*, 227, [10.1007/s11270-016-2930-z](https://doi.org/10.1007/s11270-016-2930-z), 2016.
- 450 He, J., Gong, S., Yu, Y., Yu, L., Wu, L., Mao, H., Song, C., Zhao, S., Liu, H., Li, X., and Li, R.: Air
451 pollution characteristics and their relation to meteorological conditions during 2014-2015 in major
452 Chinese cities, *Environ Pollut.*, 223, 484-496, [10.1016/j.envpol.2017.01.050](https://doi.org/10.1016/j.envpol.2017.01.050), 2017.
- 453 Hegarty, J., Mao, H., and Talbot, R.: Synoptic controls on summertime surface ozone in the northeastern
454 United States, *Journal of Geophysical Research*, 112, [10.1029/2006jd008170](https://doi.org/10.1029/2006jd008170), 2007.
- 455 Hien, P. D., Bac, V. T., Tham, H. C., Nhan, D. D., and Vinh, L. D.: Influence of meteorological
456 conditions on PM_{2.5} and PM_{2.5-10} concentrations during the monsoon season in Hanoi, Vietnam,
457 *Atmospheric Environment*, 36, 3473-3484, [10.1016/s1352-2310\(02\)00295-9](https://doi.org/10.1016/s1352-2310(02)00295-9), 2002.
- 458 Jacob, D. J., and Winner, D. A.: Effect of climate change on air quality, *Atmospheric Environment*, 43,
459 51-63, [10.1016/j.atmosenv.2008.09.051](https://doi.org/10.1016/j.atmosenv.2008.09.051), 2009.
- 460 Kinney, P. L.: Climate change, air quality, and human health, *American journal of preventive medicine*,
461 35, 459-467, [10.1016/j.amepre.2008.08.025](https://doi.org/10.1016/j.amepre.2008.08.025), 2008.
- 462 Knowland, K. E., Doherty, R. M., Hodges, K. I., and Ott, L. E.: The influence of mid-latitude cyclones
463 on European background surface ozone, *Atmospheric Chemistry and Physics*, 17, 12421-12447,
464 [10.5194/acp-17-12421-2017](https://doi.org/10.5194/acp-17-12421-2017), 2017.
- 465 Lamb, H.: British Isles weather types and a register of the daily sequence of circulation patterns, *Geophys.*
466 *Mem.*, 116, 1861-1971, 1972.
- 467 Li, K., Jacob, D. J., Liao, H., Shen, L., Zhang, Q., and Bates, K. H.: Anthropogenic drivers of 2013–2017
468 trends in summer surface ozone in China, *Proceedings of the National Academy of Sciences*, 116, 422-
469 427, [10.1073/pnas.1812168116](https://doi.org/10.1073/pnas.1812168116), 2019.
- 470 Liao, Z., Gao, M., Sun, J., and Fan, S.: The impact of synoptic circulation on air quality and pollution-
471 related human health in the Yangtze River Delta region, *The Science of the total environment*, 607-608,
472 838-846, [10.1016/j.scitotenv.2017.07.031](https://doi.org/10.1016/j.scitotenv.2017.07.031), 2017.
- 473 Liu, Y., Franklin, M., Kahn, R., and Koutrakis, P.: Using aerosol optical thickness to predict ground-
474 level PM_{2.5} concentrations in the St. Louis area: A comparison between MISR and MODIS, *Remote*
475 *Sens. Environ.*, 107, 33-44, [10.1016/j.rse.2006.05.022](https://doi.org/10.1016/j.rse.2006.05.022), 2007.
- 476 Liu, Y., He, K. B., Li, S. S., Wang, Z. X., Christiani, D. C., and Koutrakis, P.: A statistical model to
477 evaluate the effectiveness of PM_{2.5} emissions control during the Beijing 2008 Olympic Games, *Environ.*
478 *Int.*, 44, 100-105, [10.1016/j.envint.2012.02.003](https://doi.org/10.1016/j.envint.2012.02.003), 2012.
- 479 Lu, X., Hong, J., Zhang, L., Cooper, O. R., and Zhang, Y.: Severe Surface Ozone Pollution in China: A
480 Global Perspective, *Environmental Science & Technology Letters*, 5, [acs.estlett.8b00366-](https://doi.org/10.1021/acs.estlett.8b00366), 2018.
- 481 Ma, Z., Xu, J., Quan, W., Zhang, Z., Lin, W., and Xu, X.: Significant increase of surface ozone at a rural
482 site, north of eastern China, *Atmospheric Chemistry & Physics*, 16, 3969-3977, 2016.



483 Pope, R. J., Butt, E. W., Chipperfield, M. P., Doherty, R. M., Fenech, S., Schmidt, A., Arnold, S. R., and
484 Savage, N. H.: The impact of synoptic weather on UK surface ozone and implications for premature
485 mortality, *Environmental Research Letters*, 11, 124004, 10.1088/1748-9326/11/12/124004, 2016.
486 Robeson, S. M., and Steyn, D. G.: Evaluation and comparison of statistical forecast models for daily
487 maximum ozone concentrations, *Atmospheric Environment Part B Urban Atmosphere*, 24, 303-312,
488 1990.
489 Russo, A., Trigo, R. M., Martins, H., and Mendes, M. T.: NO₂, PM₁₀ and O₃ urban concentrations and
490 its association with circulation weather types in Portugal, *Atmospheric Environment*, 89, 768-785,
491 10.1016/j.atmosenv.2014.02.010, 2014.
492 Santurtún, A., González-Hidalgo, J. C., Sanchez-Lorenzo, A., and Zarrabeitia, M. T.: Surface ozone
493 concentration trends and its relationship with weather types in Spain (2001–2010), *Atmospheric*
494 *Environment*, 101, 10-22, 10.1016/j.atmosenv.2014.11.005, 2015.
495 Shen, L., Mickley, L. J., and Tai, A. P. K.: Influence of synoptic patterns on surface ozone variability
496 over the eastern United States from 1980 to 2012, *Atmospheric Chemistry and Physics*, 15, 10925-10938,
497 10.5194/acp-15-10925-2015, 2015.
498 Tang, G., Wang, Y., Li, X., Ji, D., Hsu, S., and Gao, X.: Spatial-temporal variations in surface ozone in
499 Northern China as observed during 2009–2010 and possible implications for future air quality control
500 strategies, *Atmospheric Chemistry and Physics*, 12, 2757-2776, 10.5194/acp-12-2757-2012, 2012.
501 Trigo, R. M., and Dacamara, C. C.: Circulation weather types and their influence on the precipitation
502 regime in Portugal, *International Journal of Climatology*, 20, 1559-1581, 2000.
503 Wang, W. T., Primbs, T., Tao, S., and Simonich, S. L. M.: Atmospheric Particulate Matter Pollution
504 during the 2008 Beijing Olympics, *Environmental Science & Technology*, 43, 5314-5320,
505 10.1021/es9007504, 2009a.
506 Wang, Y., Hao, J., McElroy, M. B., Munger, J. W., Ma, H., Chen, D., and Nielsen, C. P.: Ozone air
507 quality during the 2008 Beijing Olympics: effectiveness of emission restrictions, *Atmospheric Chemistry*
508 *and Physics*, 9, 5237-5251, DOI 10.5194/acp-9-5237-2009, 2009b.
509 Yarnal, B.: Synoptic Climatology in Environmental Analysis A Primer, *Journal of Preventive Medicine*
510 *Information*, 347, 170-180, 1993.
511 Zhang, J. P., Zhu, T., Zhang, Q. H., Li, C. C., Shu, H. L., Ying, Y., Dai, Z. P., Wang, X., Liu, X. Y.,
512 Liang, A. M., Shen, H. X., and Yi, B. Q.: The impact of circulation patterns on regional transport
513 pathways and air quality over Beijing and its surroundings, *Atmospheric Chemistry and Physics*, 12,
514 5031-5053, 10.5194/acp-12-5031-2012, 2012.
515 Zhang, Y., Mao, H., Ding, A., Zhou, D., and Fu, C.: Impact of synoptic weather patterns on spatio-
516 temporal variation in surface O₃ levels in Hong Kong during 1999–2011, *Atmospheric Environment*, 73,
517 41-50, 10.1016/j.atmosenv.2013.02.047, 2013.
518 Zhao, W., Tang, G., Yu, H., Yang, Y., Wang, Y., Wang, L., An, J., Gao, W., Hu, B., Cheng, M., An, X.,
519 Li, X., and Wang, Y.: Evolution of boundary layer ozone in Shijiazhuang, a suburban site on the North
520 China Plain, *Journal of Environmental Sciences*, 83, 152-160, <https://doi.org/10.1016/j.jes.2019.02.016>,
521 2019.
522
523
524
525
526



527 **Tables**

528 **Table 1. Circulation patterns, ozone concentrations and meteorological conditions for 5 weather categories.**

category	type	ozone	fre	Tmax	RH	rain	TCC	ws	BLH	div	v-v	characteristics
	N	108	5.4	25.9	64.5	2.2	6	2.1	749	0.85	2.28	MDA8 O ₃ (98±6 µg m ⁻³).
	NE	94	6.4	25.5	72.1	5.0	7	2.2	637	-1.01	-0.70	Cool, moderate rain,
	E	98	4.7	25.4	70.5	3.4	6	2.1	618	-1.34	-1.85	moderate TCC, and low
N-E-S direction	SE	105	2.3	22.8	71.5	4.9	7	2.4	612	-1.25	-3.85	BLH, predominant wind
	AN	101	1.7	22.2	61.2	1.5	5	2.3	738	2.36	5.12	directions are north and east,
	ANE	88	2.4	23.1	67.9	2.3	6	2.2	681	0.79	1.53	clean air masses from inner
	AE	94	1.3	23.2	65.8	2.2	7	2.3	618	-0.10	0.12	Mongolia or the eastern
	ASE	99	1.1	22.4	71.3	2.3	7	2.2	578	1.10	0.03	ocean.
	S	112	4.1	25.4	65.7	2.2	6	2.2	642	0.28	-1.23	MDA8 O ₃ (122±8 µg m ⁻³).
	SW	131	6.2	26.5	60.3	0.6	5	2.1	716	1.81	1.34	Moderate T and BLH, lower
	W	133	5.4	26.6	58.3	1.0	5	2.2	763	2.33	2.43	RH, weak wind, sporadic
S-W-N direction	NW	124	4.2	26.8	58.7	1.6	6	2.3	835	1.66	3.45	clouds and precipitation,
	AS	120	1.4	24.8	63.3	0.7	6	2.0	641	1.76	0.54	divergence in low
	AS	114	2.6	24.5	62.2	0.7	6	1.9	666	2.53	1.02	troposphere. Prevailing
	AW	126	1.0	23.8	58.5	0.2	5	1.8	685	3.14	4.16	southerly and westerly
	AN	115	1.5	23.4	55.2	0.9	6	2.3	794	2.47	5.07	winds.
	CN	135	2.0	29.8	68.0	2.2	6	1.9	732	0.09	0.92	The hybrid of cyclone and direction types, MDA8 O ₃ (126±16 µg m ⁻³). Widespread hot, humid, a small amount of clouds and rain, comparatively high BLH.
	CNE	119	1.8	28.2	66.0	3.2	6	2.2	724	-1.15	-0.19	
	CE	109	0.8	25.4	73.6	6.4	7	2.1	559	-2.67	-3.65	
LP	CSE	103	0.7	25.1	62.6	1.4	6	2.6	725	-1.65	-0.58	
	CS	123	1.0	27.4	65.7	1.6	5	2.1	693	-0.40	-0.67	
	CS	155	2.2	29.4	62.6	1.2	5	2.3	796	0.96	0.58	
	CW	140	2.6	28.6	62.3	1.3	5	2.2	778	0.95	0.93	
	CN	124	1.5	29.2	62.4	4.5	6	2.5	853	0.12	1.26	
C		128	18.1	29.5	67.1	3.8	6	2.2	715	-1.20	-1.22	Cyclone, similar to LP.
A		96	17.5	22.3	64.5	1.5	6	2.0	632	2.54	2.66	Anticyclone, similar to N-E-S direction.

529 **Note:** Ozone, MDA8 O₃ concentration (µg m⁻³); fre, frequency of each type (%); Tmax, daily maximum
 530 temperature (°C); RH, relative humidity (%); rain, total daily precipitation (mm); TCC, total cloud cover;
 531 WS, wind speed (m s⁻¹); BLH, boundary layer height (m); div, divergence of the wind field (10⁻⁶ s⁻¹) from 1000
 532 to 850 hPa (7 levels); and v-v, vertical velocity from 1000 to 100 hPa (10⁻² Pa s⁻¹).

533 **Table 2 All parameters used in the stepwise regression and the number of cities (out of 14) for which each**
 534 **variable was selected for each weather category.**

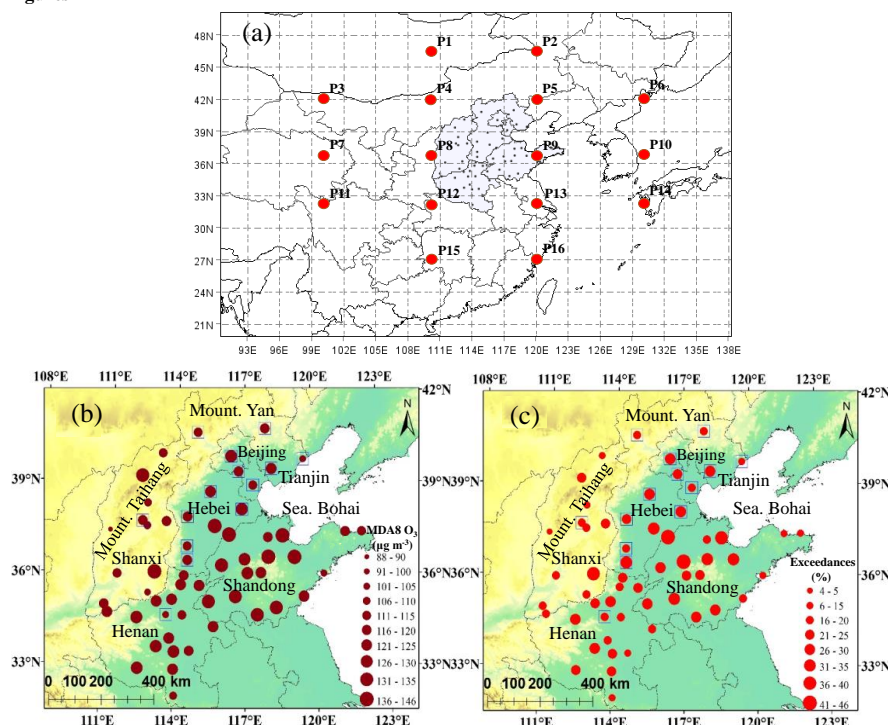
factors	N-E-S direction	S-W-N direction	LP	C	A
TCC	2	4	2	5	5
RH (%)	2	4	3	4	6
Tmax (°C)	14	14	14	14	14



rain (mm)	0	2	2	0	2
U	2	3	3	3	1
V	9	6	6	7	2
wd (°)	2	0	0	1	1
ws (m s ⁻¹)	4	1	1	0	2
pre (hPa)	0	0	0	0	0
TCC_lag	1	2	2	4	1
RH_lag (%)	11	5	5	4	4
Tmax_lag (°C)	3	0	0	1	0
rain_lag(mm)	1	0	0	0	0
U_lag	2	1	1	1	1
V_lag	4	0	0	0	4
wd_lag (°)	0	0	0	0	0
ws_lag (m s ⁻¹)	1	3	3	1	4
pre_lag (hPa)	1	0	0	1	1

535 Note: TCC, RH, Tmax, rain, U, V, wd, ws and pre are total cloud cover, relative humidity, maximum
 536 temperature, precipitation, u component, v component, wind direction, wind speed and pressure, respectively.
 537 The suffix lag means the meteorological factors from the previous day.

538 Figures

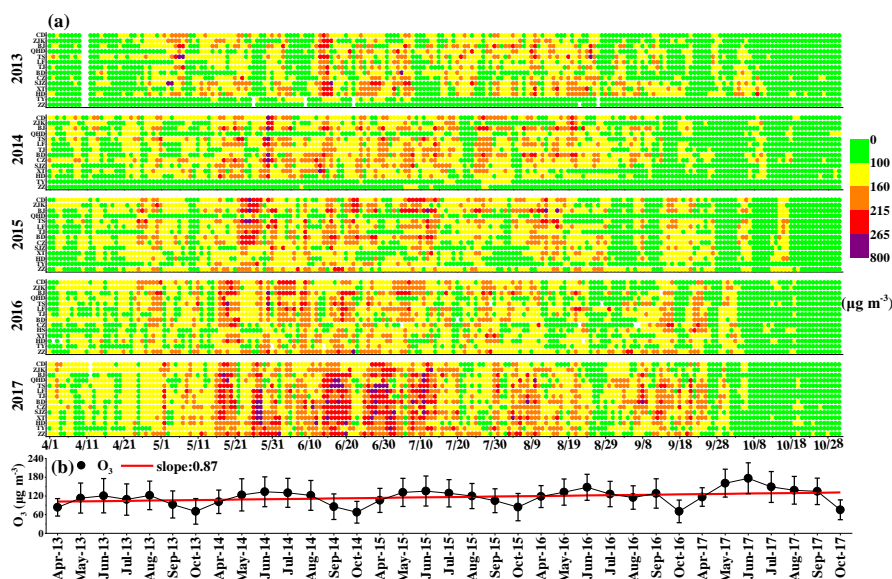


539
 540 Fig. 1. Location of North China (shaded area), all cities (black spots) and sea level pressure grids (a). The 16
 541 red points show the locations of the 5°×10° mean sea level pressure grids used for the Lamb-Jenkinson
 542 weather type classification. The spatial distributions of the maximum daily 8-h running average O₃ (MDA8



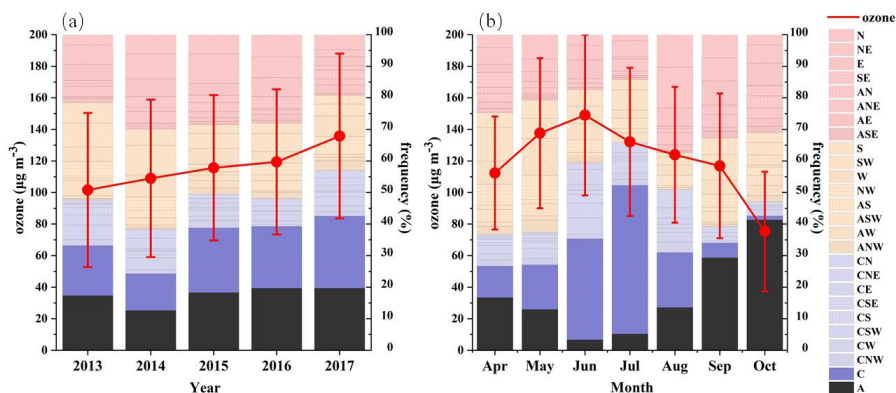
543 O₃ concentration (b) and exceedance ratios (c) for 58 cities. Statistics for 2013-2017 are shown with blue
 544 boxes, the others for 2015-2017. The base map is topography; the elevations of the Taihang Mountains are
 545 more than 1200 meters, and the Yan Mountains range from 600 to 1500 meters.

546



547

548 Fig. 2. Time series of daily MDA8 O₃ concentrations in 14 cities (north to south) (a), together with monthly-
 549 averaged concentrations and standard deviations (b), during April to October from 2013 to 2017. Five ranks
 550 represent different air-quality levels, including excellent (green spots), good (yellow), lightly polluted (orange),
 551 moderately polluted (red) and heavily polluted (purple) days with cut off concentrations of 100, 160, 215, and
 552 265 µg m⁻³. The fit line (red line) in (b) represents the increasing trend of monthly mean MDA8 O₃.

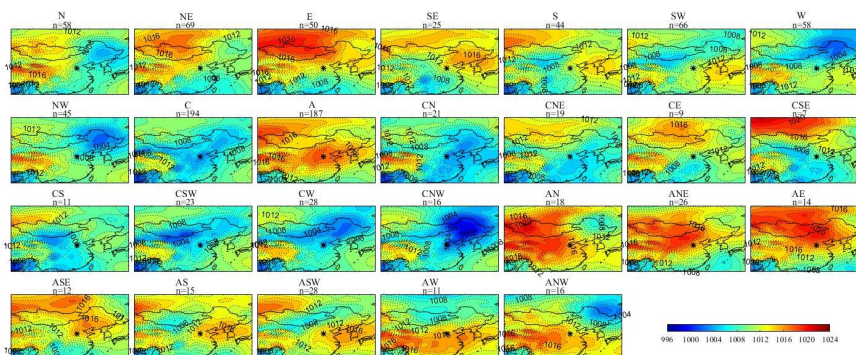


553

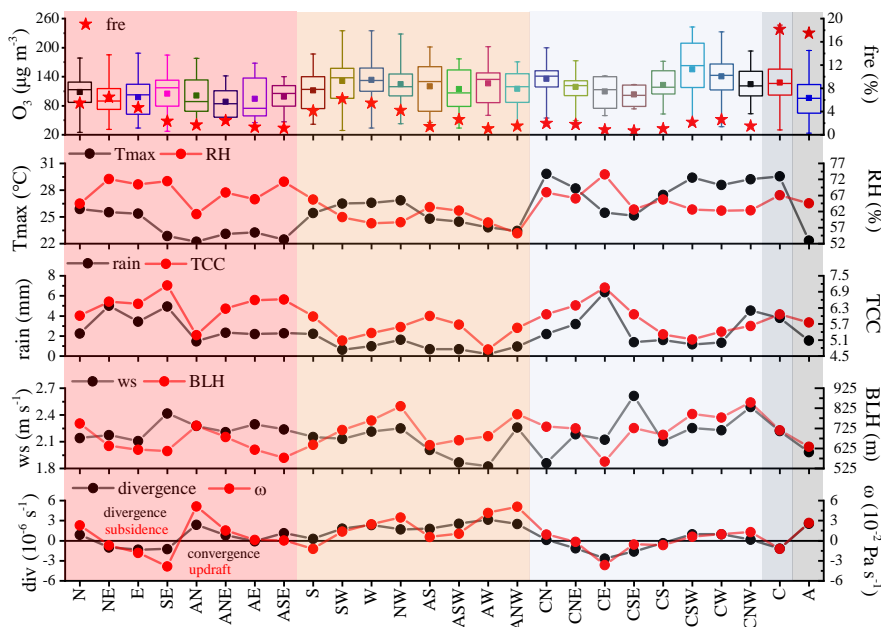
554 Fig. 3. Interannual (a) and monthly (b) averaged concentrations of ozone and frequencies of 26 circulation
 555 types from April-October 2013-2017. The red dots represent the mean values, the vertical red lines indicate
 556 the standard deviations, and stacked charts represent the percentages of various weather patterns (2013 and



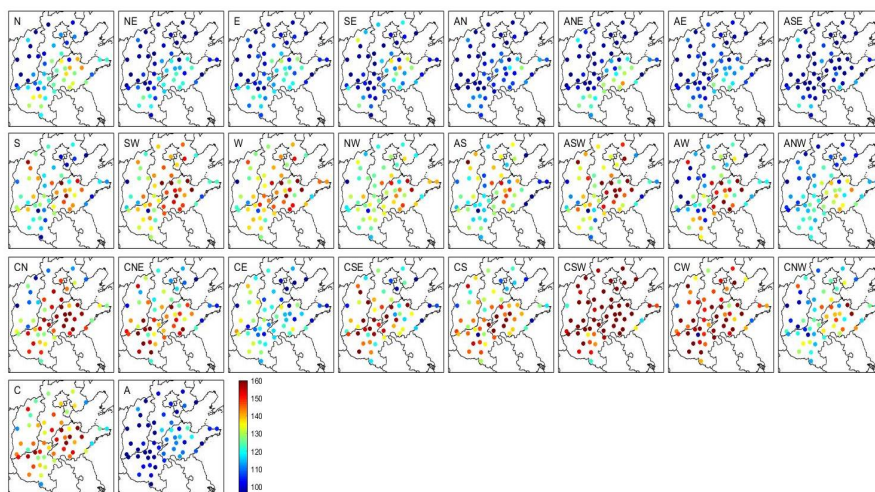
557 2014 are averaged for 14 cities, 2015-2017 are averaged for 58 cities). The pink, orange, light blue, dark blue
 558 and black areas represent the weather categories N-E-S direction, S-W-N direction, LP, C and A, respectively.



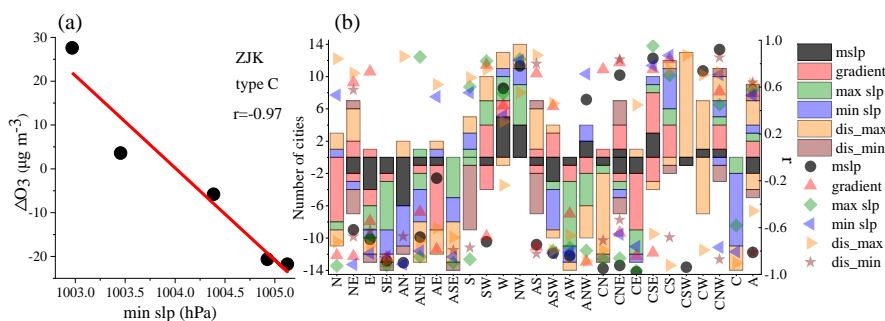
559
 560 Fig. 4. Mean surface pressure field (unit: hPa) for the 26 circulation types during April-October of 2013-2017
 561 and occurrence days (1070 days in total), ‘*’ indicates the center of North China.



562
 563 Fig. 5. Box chart of domain-averaged MDA8 O₃ concentrations, occurrence frequency of circulations (fre),
 564 and mean values of meteorological factors in 26 circulation types during April-October of 2013-2017. In box
 565 chart, the solid square indicates the mean, the horizontal lines across the box are the averages of the first,
 566 median, and the third quartiles, respectively, and the lower and upper whiskers represent the 5th and 95th
 567 percentiles, respectively. The pink, orange, light blue, dark blue and black areas represent the weather
 568 categories N-E-S direction, S-W-N direction, LP (low-pressure related circulation patterns), C (cyclone) and
 569 A (anticyclone), respectively.

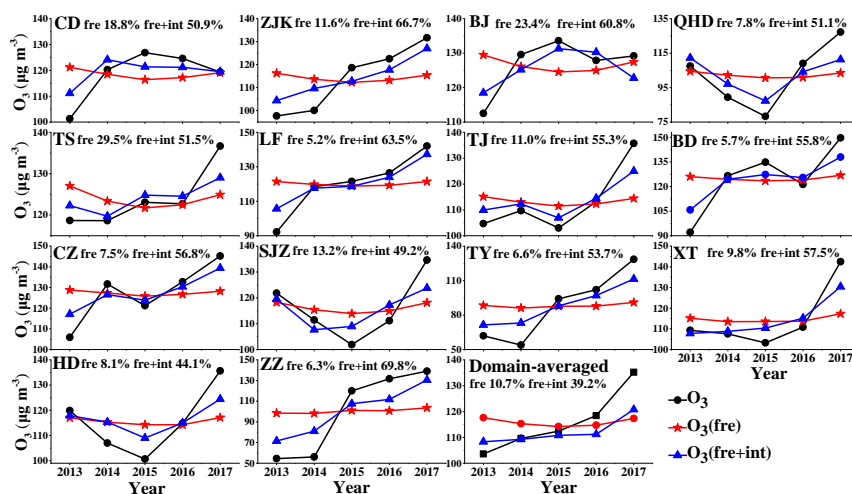


570
 571 **Fig. 6.** Spatial distribution of average MDA8 O₃ for the 26 weather types. The first, second, and third rows
 572 correspond to the weather categories N-E-S direction, S-W-N direction and LP, respectively, and the fourth
 573 row includes both categories C and A.



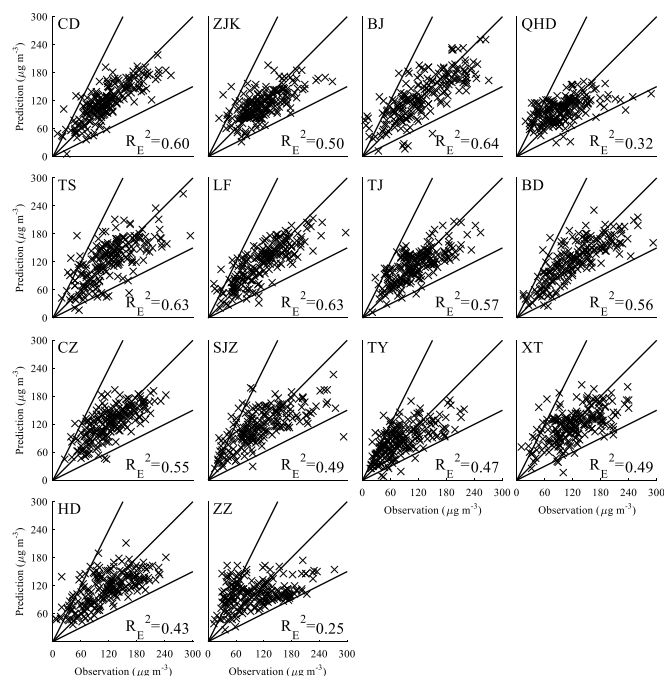
574
 575
 576 **Fig. 7.** Scatter plot of ΔO_3 versus min slp for circulation type C in ZJK (a). The red line represents the linear
 577 fitting between min slp (the ECII under circulation type C in ZJK) and ΔO_3 (the difference between the
 578 MDA8 O₃ for a given year and the corresponding 5-year average); r represents correlation coefficient. The
 579 number of cities (histogram) and averaged correlation coefficient r (points of different shapes) according to
 580 corresponding ECII under each circulation type among 14 cities (b). The number of cities with
 581 positive/negative values represents positive/negative correlations between ECII and ΔO_3 . For example, under
 582 CW controls, there are 1 and 6, and 7 cities where ECII corresponds to mslp with the positive correlation, dis
 583 max with the positive correlation, and dis max with negative correlation, respectively; and the averaged r is
 584 0.74 and 0.70, and -0.79, respectively.

585



586

587 **Fig. 8.** The inter-annual MDA8 O₃ concentration trends for observed and the reconstructed O₃ based on
 588 circulation variations in 14 cities. The black lines represent the observed inter-annual MDA8 O₃ trend,
 589 whereas the red and blue lines are the trends of reconstructed MDA8 O₃ concentrations according to the
 590 frequency-only and both frequency and intensity of circulation changes, respectively. The percentages in each
 591 city indicate the O₃ inter-annual variabilities influenced by frequency-only and by both frequency and
 592 intensity of circulation changes.



593

594 **Fig. 9.** Scatter plots of predicted versus observed MDA8 O₃ concentrations in the composite validation
 595 datasets for each city. The R_E^2 values indicate the percentage of explained variance in the composite model



596 **that contains the building and validation datasets for each city. The three black lines indicate 2:1, 1:1 and 1:2**
597 **ratios lines of predictions and observations.**

598

599